THE JOURNAL OF PHYSICAL CHEMISTRY C
A JOURNAL OF THE AMERICAN CHEMICAL SOCIETY

pubs.acs.org/JPCC Article

Stable Dimer Intermediates during Intercluster Reactions of Atomically Precise Nanoclusters

Swetashree Acharya, Jayoti Roy, Diptendu Roy, Biswarup Pathak,* and Thalappil Pradeep*

Cite This: https://doi.org/10.1021/acs.jpcc.4c07077 Read Online

ACCESS | Metrics & More | Article Recommendations | Supporting Information

ABSTRACT: Intercluster reactions involving atomically precise noble metal nanoclusters (NCs) in solution, closely resembling reactions between molecules, are important for exploring chemistry on the nanoscale. In the present study, we conducted reactions between $[Ag_{29}(1,3\text{-BDT})_{12}]^{3-}$ (1,3-BDT = 1,3-benzenedithiol) and center-doped $[MAg_{24}(2,4\text{-DMBT})_{18}]^{q-}$ (q = 1 for M = Ag, Au; and q = 2 for M = Pd, Pt; 2,4-DMBT = 2,4-dimethylbenzenethiol) NCs in solution. For the first time, we report the formation of *stable dimers*, formed between two NCs with mixed metal−ligand interfaces. The dimeric species formed were $[MAg_{53-x}BDT_{12}DMBT_{18-y}]^{3-}$ ($x \geq 0$ and $y \geq 0$), with 16 electrons in their valence shells. Here, the dimers were formed irrespective of the nature of the central atom in the NC, although the compositions were different depending on the central atom. These dimers were stable in solution for ∼2 days. The dithiol-protected $[Ag_{29}BDT_{12}]^{3-}$ part was more stable in the dimers, during fragmentation than the monothiol-protected $[MAg_{24}DMBT_{18}]^{q-}$ part. UV/vis spectroscopic and mass spectrometric analyses, along with density functional theory calculations, were used to understand the dimers. Our work highlighted the importance of the cluster interface in the stability of the dimer formed. Probing such stable dimers formed during intercluster reactions can help us understand the reaction mechanism in greater detail.

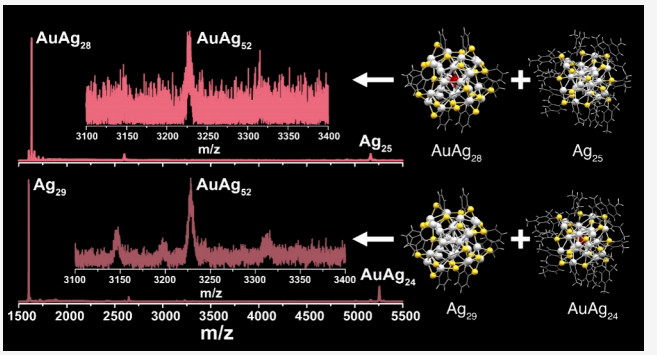

INTRODUCTION

Atomically precise noble metal nanoclusters (NCs) with metal cores and external metal−ligand shells, exhibiting quantum size effects, are widely studied molecular systems due to their unique optical, electrochemical, and catalytic properties and potential applications in various fields. They are distinctly different compared to their corresponding bulk materials and nanoparticles (NPs).[1−13] They have gained remarkable attention due to their precise composition, well-defined structures, and molecule-like behavior, which have allowed further exploration of their chemistry in greater detail.[14−22] A few NCs have been explored in terms of their reactions, leading to structural changes and also resulting in assemblies.[23−30] Earlier research on thiolate-protected noble metal NCs has predominantly focused on their synthesis, structure determination, and evaluation of essential properties.[31−36] Metal atom exchange during reactions between atomically precise NCs was identified by Krishnadas et al.[37] This type of molecular reactivity between NCs was investigated in several contexts, namely, alloying, dynamics, size homogenization, assembly, etc.[37−48] Reactions between NCs and bulk metal also occur leading to atom exchange.[49,50] We understand now that NCs react like molecules, exchanging metal atoms, ligands, and metal−ligand fragments under ambient conditions. These metal exchange reactions depend on the relative energies of doping, reduction potentials, and electron affinities of the heterometal atoms.[51−53] Understanding these molecular interactions is essential for exploring the potential applications of such NCs. The molecular reactivity of NCs has been the subject area of a few reviews.[27,41,53]

These intercluster reactions have gained popularity due to their ability to form bimetallic and trimetallic alloy NCs. For example, reactions of thiolate-protected $Au_{25}(SR)_{18}$ with $Ag_{44}(SR)_{30}$ and $MAg_{28}(S_2R)_{12}$ form such alloys.[37,38] These NCs also conserve their original structure in an intercluster alloying reaction between structurally comparable Au and Ag NCs, such as $Au_{25}(SR)_{18}$ and $Ag_{25}(SR)_{18}$.[39] In another Au−Ag alloy NC forming reaction, only metal atoms undergo exchange, without any ligand or metal−thiolate fragment exchanges.[40] Alloy NCs synthesized through intercluster reactions typically share common structural features but exhibit diverse reactivities in their substitution reactions,

Received: October 18, 2024
Revised: December 21, 2024
Accepted: December 27, 2024

depending on their metal cores, ligands, and geometries. These intercluster reactions reveal the role of the nature of the metal−ligand interface of NCs and its exchange dynamics in solution, which dictate the type and rate of exchange processes.[42,43,54] Therefore, analysis of intercluster reactions encompasses various aspects of their kinetics and thermodynamics.[44,54] Density functional theory (DFT) studies of NC reactions also offer systematic and fundamental insights that enhance the study's credibility across various fields.[45] During intercluster reactions, transient intermediate dimers were detected, such as the reaction between $[Ag_{25}(SR)_{18}]^-$ and $[Au_{25}(SR)_{18}]^-$ leading to alloy NCs.[39] In the literature, individual NCs like $Au_{25}(SR)_{18}$ are known to form homodimers or trimers in the gas phase.[55] Dimers of NCs have also been formed using linker species.[56,57] However, no stable dimers have been observed during intercluster reactions. Our motivation to explore the effect of the central atom in these reactions stemmed from our group's earlier work, which reported isotopic exchange in isotopically pure homometallic $Ag_{25}(SR)_{18}$ NCs made of ^{107}Ag and ^{109}Ag. This study revealed that the reaction between these two NCs occurred spontaneously, to attain equilibrium in the statistical distribution of the isotopes, driven by the entropy of mixing.[54] This suggests that homometallic exchange reaction platforms can further help us understand the interactions between metal NCs by avoiding enthalpy changes and varying the reaction mechanisms.

In the present report, we showed that stable dimers can form during intercluster reactions between NCs of the M_{29} and M_{25} families. The NCs used specifically were $[MAg_{28}(1,3\text{-}BDT)_{12}]^{p-}$ (1,3-BDT= 1,3-benznedithiol) hereafter referred to as $[MAg_{28}L_{12}]^{p-}$ (and abbreviated as $M@I^{p-}$) (p = 3, M = Ag,Au, and p = 4, M = Pd,Pt) and $[MAg_{24}(2,4\text{-}DMBT)_{18}]^{q-}$ (2,4-DMBT = 2,4-dimethylbenzenethiol) hereafter referred to as $[MAg_{24}L'_{18}]^{q-}$ (and abbreviated as $M@II^{q-}$) (q = 1 for M = Ag,Au, and q = 2 for M = Pd,Pt), with different ligands and central metal atoms. For a simplified description of NCs, Ag_{29}, Ag_{25}, Ag_{53}, and Ag_{54} systems with their ligands are abbreviated as Ag@I, Ag@II, Ag@III, and Ag@IV. For explicitly specifying the central atom, we use notations like Ag@I and Au@I to represent Ag_{29} and $AuAg_{28}$, respectively. The parent NCs and reaction products were characterized using optical absorption spectroscopy (UV/vis) and electrospray ionization mass spectrometry (ESI MS). The reactions typically produce dimeric entities with AgL′ losses. The dimeric species formed were heterodimers of $M@I^{p-}$ and $M@II^{q-}$, which is unusual for intercluster reactions. Density functional theory (DFT) calculations further confirmed the stability of these NC dimers, suggesting that dithiol (L) protection enhances the interface stability.

EXPERIMENTAL SECTION

Chemicals and Solvents. We purchased silver nitrate ($AgNO_3$) from Rankem Chemicals and 2,4-dimethylbenzenethiol (DMBT) (≥95%), 1,3-benzenedithiol (BDT) (≥99%), tetraphenylphosphonium bromide (PPh_4Br), triphenylphosphinegold(I) chloride ($AuPPh_3Cl$), palladium acetate ($Pd(OAc)_2$), chloroplatinic acid (K_2PtCl_4), sodium borohydride ($NaBH_4$, 95%), and triethylamine (Et_3N) from Sigma-Aldrich. Spectrochem supplied triphenylphosphine (PPh_3, 98%). Rankem supplied dichloromethane (DCM), dimethylformamide (DMF), acetonitrile (ACN), acetone (ACE), and methanol (MeOH); all of them were of HPLC quality. All compounds were used without additional purification.

Synthesis of $Ag_{25}(DMBT)_{18}$ (Ag@II). The NC was synthesized using a slightly altered version of the Brust method that was reported earlier.[58] Around 38 mg of $AgNO_3$ was dissolved in 2 mL of MeOH, and roughly 17 mL of DCM was added. After adding about 90 μL of DMBT to this solution, a thick yellow mixture was produced. Approximately 6 mg of PPh_4Br in 0.5 mL of MeOH was added after 5 min, followed by the addition of 15 mg $NaBH_4$ in 0.5 mL ice-cold water, after 20 min into the reaction mixture. The reaction mixture was stirred for approximately 8 h and then aged for 24 h. The reaction mixture produced a dark brown solution that was centrifuged. The supernatant was collected in a round-bottom flask and concentrated using a rotary evaporator to a volume of 2 mL. After that, the NC was precipitated by adding excess MeOH and then repeatedly cleaned with MeOH. Finally, the NC was extracted by dissolving the precipitate in DCM.

Synthesis of $AuAg_{24}(DMBT)_{18}$ (Au@II). Pure Au-doped Au@II was synthesized by using a modified version of a previously published galvanic exchange process.[17] Around 5 mg of pure Ag_{25} was dissolved in 5 mL DCM and placed in a 10 mL glass bottle with 0.1 mg of $AuPPh_3Cl$ in 1 mL DCM. The reaction was kept stirring for about 2−3 h. After the NC solution had formed, DCM was evaporated in a rotary evaporator and then cleaned with MeOH. The NCs were extracted with DCM.

Synthesis of $MAg_{24}(DMBT)_{18}$ (M = Pd, Pt) (M@II). For the synthesis of Pd@II and Pt@II, we adhered to a previously published protocol.[59] First, approximately 10 mg of $AgNO_3$ and approximately 10 mg of $Pd(OAc)_2$ or K_2PtCl_4 were dissolved in 5 mL of MeOH along with 9 mL of DCM, respectively. Subsequently, around 10 μL of DMBT in 0.5 mL of DCM was added to the reaction mixture, followed by approximately 10 mg of PPh_4Br in 0.5 mL of DCM addition. The NCs were formed when 40 mg of $NaBH_4$ in 0.5 mL of ice-cold water was introduced to the reaction mixture after 20 min, followed by the addition of 50 μL of triethylamine after 5 min with overnight stirring. The formed NC solution was evaporated, and the residue was washed with MeOH. The NCs were extracted with DCM.

Synthesis of $Ag_{29}(BDT)_{12}(PPh_3)_4$ (Ag@I). The NC was synthesized by adopting an already-reported method.[60] First, around 20 mg of $AgNO_3$ was dissolved in 5 mL of MeOH, and then, 9 mL of DCM was added. After a few minutes, approximately 13.5 μL of BDT in 0.5 mL of DCM was added to the solution. Then, after 5 min of stirring in the dark, nearly 200 mg of PPh_3 in 0.5 mL of DCM was added to the mixture, and next, 0.5 mL of an ice-cold aqueous solution of 11 mg of $NaBH_4$ was added, which immediately changed the color of the solution to dark brown. The reaction was kept for 3 h under dark conditions. Then, the red precipitate was collected by centrifugation. The NC was washed several times with MeOH, and the residue was dissolved in DMF. The reddish-orange NCs were collected after the removal of unwanted byproducts.

Synthesis of $MAg_{28}(BDT)_{12}(PPh_3)_4$(M@I where M = Au, Pd, or Pt). The ligand exchange-induced structural/size transformation (LEIST)[61] method was used for the synthesis of M@I.[38] M@II was taken in DCM as the precursor, and then, 1 μL of BDT and 50 mg of PPh_3 were added to the reaction mixture, which was kept in the dark for 1 h. After that,

https://doi.org/10.1021/acs.jpcc.4c07077
J. Phys. Chem. C XXXX, XXX, XXX−XXX

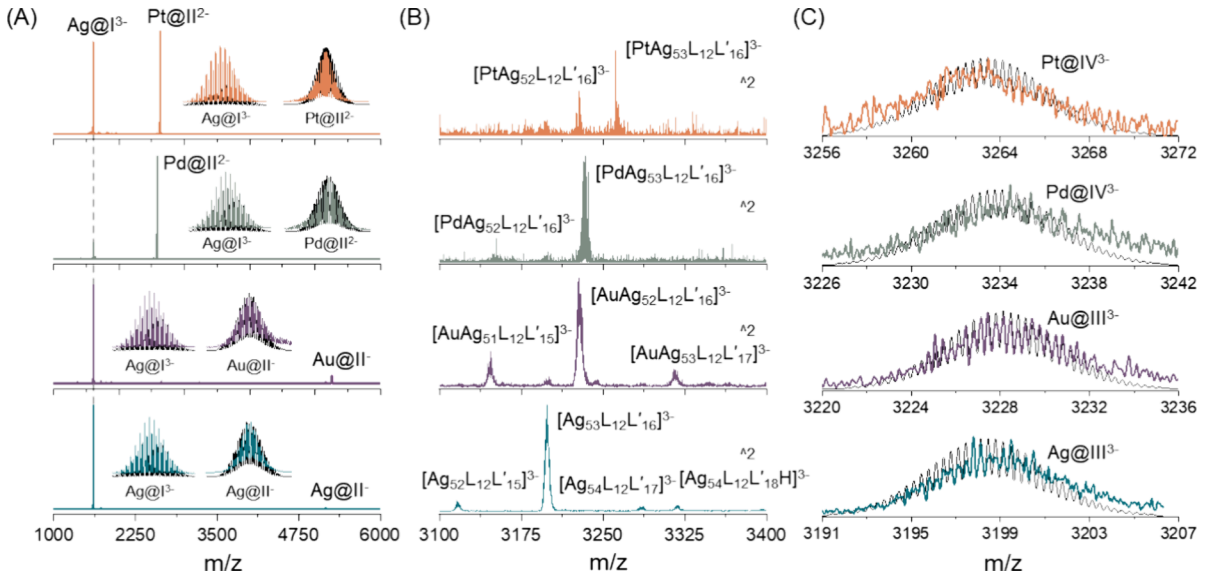

Figure 1. Formation of the dimeric species in all four cases of reaction between $Ag@I^{3-}$ and $M@II^{q-}$ (M= Ag, Au, Pd, Pt), in 1:1 ratio, in acetonitrile solvent. Spectra were collected 5 min after mixing the clusters. (A) Full range mass spectra of the reaction mixture and inset show the isotopic distribution of both the parent NCs in the reaction mixture. (B) Dimer region and (C) theoretical and experimental isotopic distributions of the most intense dimeric species in each case. In $Pd@IV^{3-}$ and $Pt@IV^{3-}$, the peaks were not resolved clearly due to the poor intensity.

DCM was evaporated, and the formed NC was washed with MeOH several times. Then, the NCs were extracted in DMF and used for further characterization.

Characterization. Optical absorption spectra of the samples were collected by using a PerkinElmer Lambda 25 spectrometer. About 100 μM of purified NCs and the mixture of NCs (in 3 mL of ACN) were used for measuring the UV/vis spectra. ESI MS of samples were measured using a Waters Synapt G2-Si high-resolution mass spectrometer. About 1 μM purified NCs and a mixture of NCs (in 1 mL of ACN) were used for measuring the mass spectra.

Computational Details. The optimization of the NCs has been performed using the projector-augmented-wave (PAW) method, as implemented in the Vienna ab initio simulation package (VASP).[62−64] For the description of the exchange-correlation potential, the generalized gradient approximation of Perdew−Burke−Ernzerhof (GGA-PBE) is used.[65] Moreover, to expand the electronic wave function, 470 eV plane wave cutoff energy was used.[62] The convergence criteria are set as 0.05 eV/Å for the force and 1×10^{-2} eV for the electronic energy minimization. For all the calculations, van der Waals correction has been included.

RESULTS AND DISCUSSION

Reaction between $Ag@I^{p-}$ with $M@II^{q-}$. We have synthesized the NCs: $M@I^{p-}$ and $M@II^{q-}$ (M = Ag/Au/Pd/Pt) using the previously reported methods[17,38,58−60] and characterized them using UV/vis and ESI MS, as shown in Figures S1 and S2, respectively. These NCs were used as precursors for the reaction, which form anionic dimers detected using ESI MS. Initially, $Ag@I^{3-}$ and $Ag@II^{-}$ were selected in view of their monometallic composition. However, this prevents us from observing common occurrences of metal exchanges that is typically observed during heterometallic intercluster reactions.[41] As noted before, isotopically pure clusters have shown atom exchanges in monometallic clusters.[54] In our later study, we replaced the central Ag atom in $Ag@II^{-}$ with a single Au, Pd, or Pt, to investigate the reactions of $Ag@I^{3-}$ and $M@II^{q-}$ (where M = Au, Pd, Pt), by which we thought to understand the impact of central atom on intercluster reaction. We noticed that the reactions of $Ag@I^{3-}$ and $M@II^{q-}$ form a series of intermediate species in the range m/z 3000−3500. These species correspond to dimeric entities formed in the reaction mixture, as shown in Figure 1. In Figure 1A, the full range mass spectra for all four reaction mixtures of the NCs are shown with the isotopic distribution of parent NCs in the insets, and in Figure 1B, the expanded m/z region is presented where the dimeric species formed are shown. Figure 1C compares the experimental isotopic distribution of the most intense peak among the dimeric species with its theoretical mass spectrum, showing an exact match between them.

In the reaction between $Ag@I^{3-}$ and $Ag@II^{-}$, the most abundant species was identified as $[Ag_{53}L_{12}L'_{16}]^{3-}$ (abbreviated as $Ag@III^{3-}$) at m/z 3198 formed due to the loss of $AgL'_2{}^{-}$ from $[Ag_{54}L_{12}L'_{18}]^{4-}$. $[Ag_{54}L_{12}L'_{18}]^{4-}$ is the complete dimer made of the two NCs, $Ag@I^{3-}$ and $Ag@II^{-}$, which was not directly observed in ESI MS. Species like $[Ag_{52}L_{12}L'_{15}]^{3-}$ and $[Ag_{54}L_{12}L'_{17}]^{3-}$ were found at m/z 3117 and 3280, formed due to the loss of $Ag_2L'_3{}^{-}$ and L'^{-} from $[Ag_{54}L_{12}L'_{18}]^{4-}$, respectively. Additionally, we observed that $[Ag_{54}L_{12}L'_{18}H]^{3-}$ at m/z 3326 formed due to an H^+ attachment to the complete dimer that might have been formed by the linking of the two NCs, $Ag@I^{3-}$ and $Ag@II^{-}$ in the ESI source. A detailed ESI MS study in the dimer region is shown in Figure S3. Note that the integral dimer $[(Ag@I)(M@II)]^{(q+3)-}$ that should be formed by the two NCs, $Ag@I^{3-}$ and $M@II^{q-}$ used for the reaction, was not observed in the ESI MS in any case. Dimeric species with 16 e^- species appear with high intensity, which is attributed to the higher stability of the super atomic electronic structure. ESI MS of the reaction mixture of $Ag@I^{3-}$ and $Au@II^{-}$ also yielded a range of dimeric species with a 3-charge state. The species were identified as $[AuAg_{52}L_{12}L'_{16}]^{3-}$ (abbreviated as $Au@III^{3-}$), $[AuAg_{51}L_{12}L'_{15}]^{3-}$, and $[AuAg_{53}L_{12}L'_{17}]^{3-}$ at m/z 3228, 3146, and 3309 formed due to loss of $AgL'_2{}^{-}$, $Ag_2L'_3{}^{-}$, and L'^{-}, respectively, from the integral cluster dimer,

https://doi.org/10.1021/acs.jpcc.4c07077
J. Phys. Chem. C XXXX, XXX, XXX−XXX

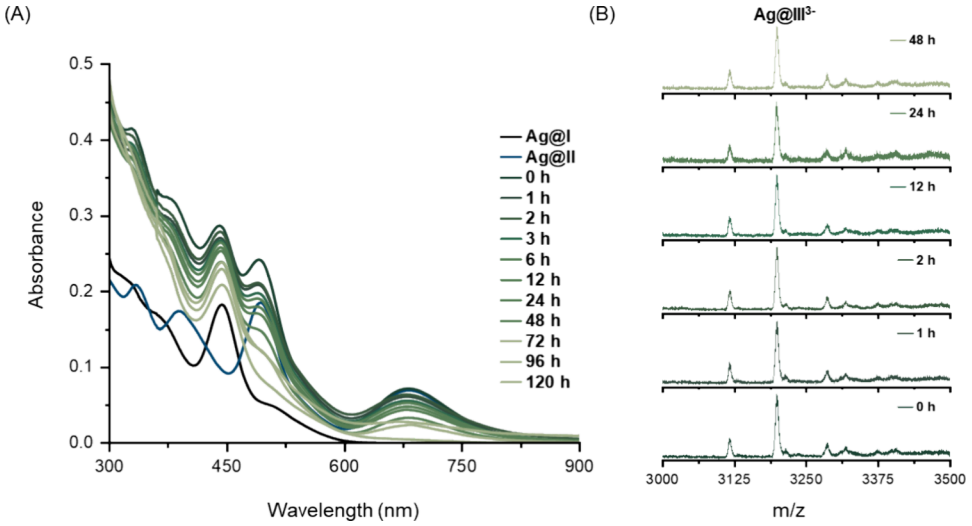

Figure 2. Monitoring the reaction mixture of $Ag@I^{3-}$ and $Ag@II^{-}$ by UV/vis and ESI MS to check the stability of the species formed during the reaction. (A) UV/vis study for the reaction mixture shows mixed features of both the parent NCs up to 48 h and subsequently the mixed nature started disappearing. (B) ESI MS study showing the stability of the dimers up to 48 h.

$[AuAg_{53}L_{12}L'_{18}]^{4-}$. Detailed ESI MS is shown in Figure S4. The most intense peak in the mass spectrum corresponds to species $Au@III^{3-}$ at m/z 3228.

ESI MS of the reaction mixture of $Ag@I^{3-}$ and $Pd@II^{2-}$ resulted in a range of dimeric species in the m/z 3100−3400 window, with a 3-charge state. All the observed species were part of the integral cluster dimer $[PdAg_{53}L_{12}L'_{18}]^{5-}$, which was not observed in ESI MS. They were assigned to be $[PdAg_{53}L_{12}L'_{16}]^{3-}$ (abbreviated as $Pd@IV^{3-}$), $[PdAg_{52}L_{12}L'_{16}]^{3-}$ (abbreviated as $Pd@III^{3-}$), and $[PdAg_{52}L_{12}L'_{15}]^{3-}$ at m/z 3234, 3198, and 3152, respectively. These species result from the sequential loss of two L′ species, AgL'_2, and AgL'_3 from the real dimer $[PdAg_{53}L_{12}L'_{18}]^{5-}$. Here, an M_{54} (from Ag_{29} + $PdAg_{24}$) analogue was observed with the loss of two ligands forming the 16 e^- species, i.e., $Pd@IV^{3-}$ with the highest intense peak in MS. The $Pd@III^{3-}$ is a 15 e^- species showing less intensity, in comparison to the 16 e^- species. Detailed ESI MS data for the reaction in the dimer region are shown in Figure S5. Similarly, ESI MS of the reaction mixture of $Ag@I^{3-}$ and $Pt@II^{2-}$ obtained several dimeric species in the m/z 3100−3400 range, with a 3-charge state. The observed species were assigned to $[PtAg_{53}L_{12}L'_{16}]^{3-}$ (abbreviated as $Pt@IV^{3-}$), $[PtAg_{52}L_{12}L'_{16}]^{3-}$ (abbreviated as $Pt@III^{3-}$), and $[PtAg_{52}L_{12}L'_{15}]^{3-}$ at m/z 3263, 3227, and 3181, respectively. These species result from the sequential loss of two L′, AgL'_2, and AgL'_3 from the integral dimer, $[PtAg_{53}L_{12}L'_{18}]^{5-}$. Here also, an M_{54} (i.e., Ag_{29} + $PtAg_{24}$) analogue was observed with the loss of two ligands forming 16 e^- species, i.e., $Pt@IV^{3-}$, giving the highest intense peak in MS. The ion $Pt@III^{3-}$ is a 15 e^- species showing less intensity in MS in comparison to the 16 e^- species. Detailed ESI MS of the dimer region is shown in Figure S6.

Dimer Formation and Stability. The formation of dimers occurs in solution, and they are detected in the gas phase by ESI MS. To determine whether the dimeric ions are formed only in the gas phase or in solution, we studied the ion formation by varying the probe distance (from capillary to cone orifice) from 4 to 12 mm. It is known that ions can retain their solution phase structures when the probe tip is close to the cone aperture where high field conditions are present. However, as the distance between the spray needle and the entrance orifice increases (under low field conditions), the population of gas-phase ions grows. This phenomenon can be explained by the charge residue and ion evaporation models, which describe how ions are generated during electrospray.[66,67] Figure S7 shows the ESI MS and arrival times of the stable dimeric species $Ag@III^{3-}$ after passing through the ion mobility cell at different probe distances. The arrival time distribution indicates that $Ag@III^{3-}$ exists as only one isomer in the gas phase. As the probe distance increases from 4 to 12 mm, in 2 mm increments, the ion intensity decreases from 7.6 × 10^6 to 1.8 × 10^5, but no other changes are observed in the arrival time distribution of the ions, indicating that the dimers formed in solution are stable and they consist of one isomer, with no structural changes occurring during the transition from solution phase to gas phase.

The UV/vis spectra of the reaction mixture exhibited a combination of peaks of both parent NCs, indicating the integrity of parent NCs throughout the reaction. At different time intervals of all the reactions between $Ag@I^{3-}$ and $M@II^{q-}$, the UV/vis spectra were measured to confirm the stability of the species (see Figure S8). The dimers get formed soon after we mix both the parent NCs in solution at ambient conditions and once the dimer gets formed, it is stable enough to be observed throughout the reaction, unlike the dimers reported in earlier intercluster reactions, which lasted only for a few minutes.[39] A detailed kinetic study of intercluster metal atom exchange reactions between $[Ag_{25}(SR)_{18}]^-$ and $[Au_{25}(SR)_{18}]^-$ leading to the entire series of monomeric and dimeric products $[Ag_mAu_{25-m}]^-$ (m = 1−24) and $[Ag_mAu_{50-m}]^{2-}$ (m = 0−50), respectively, showed the dimers for up to 1 h.[44] In contrast, MAg_{53-x} dimers formed between Ag_{29} and MAg_{24} NCs in the present study are observable for up to 48 h, persisting in solution unless one of the parent nanoclusters degrades. The stability of the reaction mixture was studied with ESI MS. All the dimeric species in the case of reaction between $Ag@I^{3-}$ and $Ag@II^{-}$ were stable up to 2 days from the start of the reaction (see Figure S9). Similarly, the stability of the dimeric species formed in the case of reaction of $Ag@I^{3-}$ with $Au@II^{-}$, $Pd@II^{2-}$, and $Pt@II^{2-}$ was monitored for 2 h from the start of the reaction in ESI MS, and the data are shown in Figures S10−S12, respectively. We did not observe any further atom

https://doi.org/10.1021/acs.jpcc.4c07077
J. Phys. Chem. C XXXX, XXX, XXX−XXX

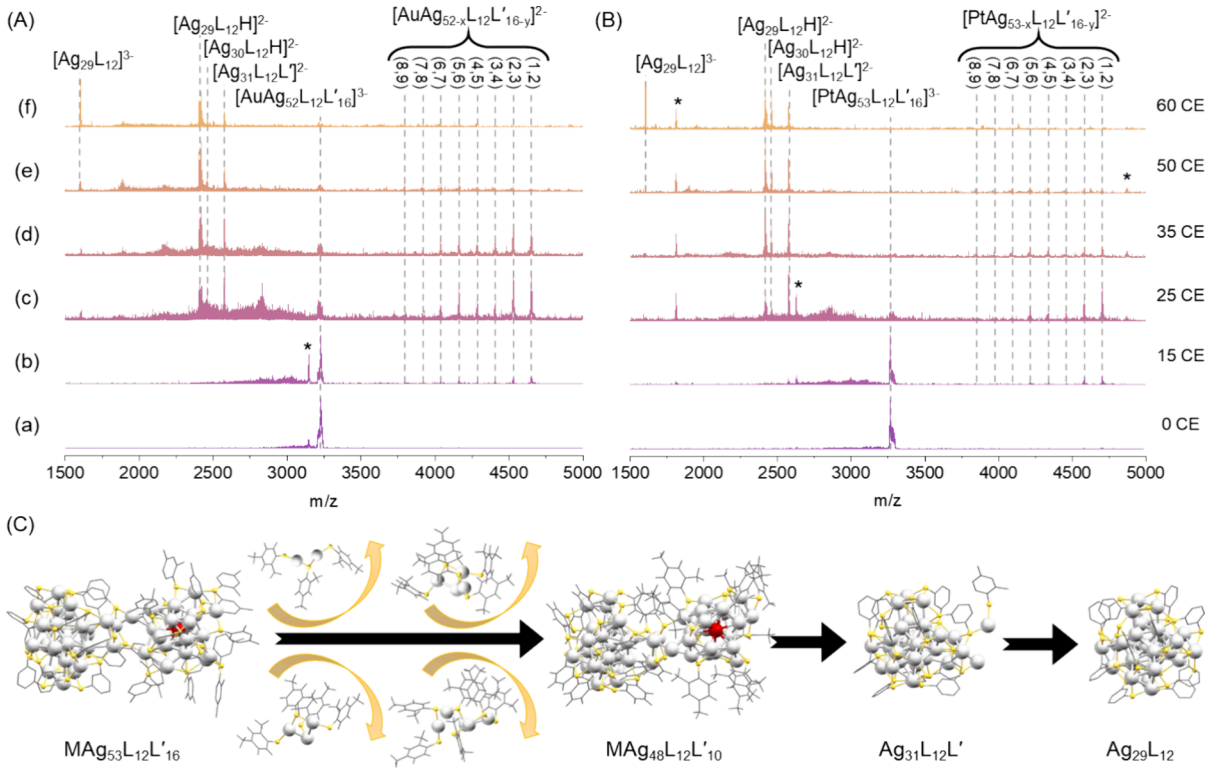

Figure 3. Collision-induced dissociation of the formed dimers, (A) $[AuAg_{52}L_{12}L'_{16}]^{3-}$ ($Au@III^{3-}$) and (B) $[PtAg_{53}L_{12}L'_{16}]^{3-}$ $Pt@IV^{3-}$, showing similar fragmentation patterns. (C) Schematic of the fragmentation pathways followed by the dimers, $[MAg_{53}L_{12}L'_{16}]^{3-}$ ($M@IV^{3-}$) (where M = Ag/Au/Pd/Pt and is shown as a red atom). In parts A and B, the label * denotes additional peaks that emerged during fragmentation. These are explained in detail in the section on the Dissociation Pathways of Dimers.

transfer during the reactions. This suggests that the interactions of the NCs and the stability of dimers depend on the chosen NC systems. The dimeric species formed are stable even when we apply external stimuli, such as heat or ultrasound, to the reaction mixture, as shown in the case of the reaction between $Ag@I^{3-}$ and $Au@II^{-}$ (see Figures S13 and S14). With these reactions and given external stimuli, we anticipated that the central atom of $M@II^{q-}$ would exchange with the center of $Ag@I^{3-}$, but this exchange did not occur. Instead, to our surprise, the dimeric species formed through these reactions remained stable. The stability of the species formed in the reaction of $Ag@I^{3-}$ and $Ag@II^{-}$ is shown in Figure 2. In Figure 2A, the change in UV/vis spectra with time is shown in comparison to the parent $Ag@I^{3-}$ and $Ag@II^{-}$. Absorption features for both the NCs were present in the reaction mixture and remained stable for up to 48 h. In Figure 2B, the MS studies suggest the stability of the dimer $Ag@III^{3-}$ along with other dimeric species formed in the reaction of $Ag@I^{3-}$ and $Ag@II^{-}$, for up to 2 days. Afterward, only one of the parent NCs ($Ag@II^{-}$) remained stable in the ACN solution, with no detectable peaks for the dimers or the parent $Ag@I^{3-}$ NC. The MAg_{53-x} dimers observed in this work were formed exclusively in the presence of their precursors, Ag_{29} and MAg_{24} NCs, and could not be isolated from the reaction mixture. Again, by varying the concentration of the parent NCs, we observed that the dimeric species are more intense for a higher concentration of $Ag@I^{3-}$ used for the reaction. This is shown in the reaction between $Ag@I^{3-}$ and $Au@II^{-}$ in Figure S15.

Dissociation Pathways of Dimers. To better understand dimer formation, we trapped the dimeric species in the trap cell and performed collision-induced dissociation (CID) on them by applying increasing collision energy (CE) (in the laboratory unit) by using argon gas. The dissociation pattern of the trapped dimers was recorded to analyze the fragmentation pathways. CID for $Ag@III^{3-}$, $Au@III^{3-}$, $Pd@IV^{3-}$, and $Pt@IV^{3-}$ resulted in similar fragmentation patterns. The onset of fragmentation occurs at 15 CE, when the trianionic dimeric species $[MAg_{53-x}L_{12}L'_{16}]^{3-}$ (x = 1 for Ag and Au and 0 for Pd and Pt) dissociates to give a series of monoanionic species, $[AgL'_2]^{-}$, $[Ag_2L'_3]^{-}$, $[Ag_3L'_4]^{-}$, and so on. Additionally, dianionic species $[MAg_{53-x}L_{12}L'_{16-y}]^{2-}$ are formed, with (x,y) values of (2,3), (3,4), (4,5), and so on, where M is Ag or Au and the values of (x,y) are (1,2), (2,3), (3,4), and so on where M is Pd or Pt. This is shown in Figure 3, where Figure 3A shows the fragmentation of $Au@III^{3-}$ and Figure 3B shows the fragmentation of $Pt@IV^{3-}$. They are the most intense peaks for the dimers in the reactions of $Ag@I^{3-}$ with $Au@II^{-}$ and $Pt@II^{2-}$, respectively. In Figure 3A, the * denotes $[AuAg_{51}L_{12}L'_{15}]^{3-}$, which was trapped along with $[AuAg_{52}L_{12}L'_{16}]^{3-}$ during mass selection for fragmentation. In Figure 3B, label * denotes $[PtAg_{24}L'_{18}]^{2-}$ at m/z 2627, $[PtAg_{23}L'_{16}]^{-}$ at m/z 4872, and $[PtAg_9L_4S_3]^{-}$ at m/z 1810 observed during the fragmentation of the dimer, $[PtAg_{53}L_{12}L'_{16}]^{3-}$. Detailed fragmentation pathways for the dimers formed in all four reactions along with lower range mass spectra from m/z 100 to 1500 are given in Figures S16–S19.

With an increase in CE, more AgL' fragments start dissociating from the dimers and the fragmented $[MAg_{53-x}L_{12}L'_{16-y}]^{2-}$ species. At 25 CE, we observe the onset of the fragment $[Ag_{31}L_{12}L']^{2-}$ which was formed due to

https://doi.org/10.1021/acs.jpcc.4c07077
J. Phys. Chem. C XXXX, XXX, XXX−XXX

the dissociation of M@II^{q-} from the dimer leaving an $[Ag_2L']^+$ attached to Ag@I^{3-} NC. With a further increase to 40−50 CE, we could only observe species corresponding to $[Ag_{30}L_{12}H]^{2-}$ which may subsequently fragment to become $[Ag_{29}L_{12}H]^{2-}$. At 50−60 CE, we discovered the reappearance of $[Ag_{29}L_{12}]^{3-}$ likely to be generated from $[Ag_{29}L_{12}H]^{2-}$ by losing one H^+. To show the reappearance of $[Ag_{29}L_{12}]^{3-}$, the expanded region of the mass spectrum is shown in Figures S20−S23, for all four cases of dimer fragmentation. This fragmentation behavior highlights the stability of Ag@I^{3-} in the gas phase and its role in the formation of stable dimeric species. A schematic representation of this process is provided in Figure 3C, representing the general fragmentation pathways followed by the dimers M@III^{3-} and M@IV^{3-}.

In all four cases of dimer fragmentation, we consistently observed the reappearance of Ag@I^{3-}. Figure 4 shows the

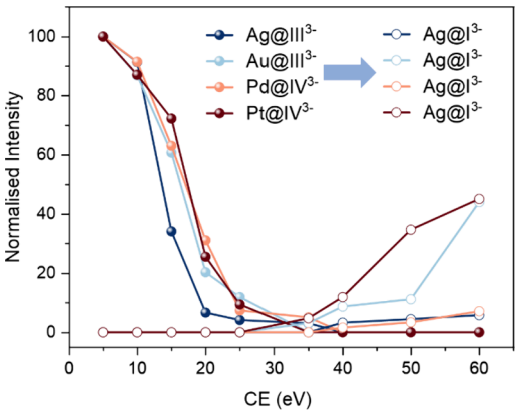

Figure 4. Comparison of the variation of normalized intensity of the dimer species Ag@III^{3-}, Au@III^{3-}, Pd@IV^{3-}, and Pt@IV^{3-} with increasing CE and the appearance of Ag@I^{3-} after 30−40 CE in each fragmentation process.

variation in relative intensities of different dimers and Ag@I^{3-} observed during the fragmentation of each dimer, plotted as a function of the CE in the trap cell. As CE increases, the intensities of the dimers, M@III^{3-} (where M = Ag, Au) and M@IV^{3-} (where M = Pd, Pt), gradually decrease, while the intensity of the fragment ion, Ag@I^{3-} increases steadily after 30 CE. These data suggest that the dimers were initially formed by the interaction of Ag@I^{3-} and M@II^{q-}, which were likely brought closer together on the NC surface through C−H···π interactions. While fragmenting the dimers of Au@III^{3-} and Pt@IV^{3-}, a higher amount of Ag@I^{3-} was observed as compared to Ag@III^{3-} and Pd@IV^{3-}, respectively, indicated by their relative intensity in Figure 4. The higher intensity of Ag@I^{3-} observed during the fragmentation of Au@III^{3-} and Pt@IV^{3-} indicates a stronger and more stable interaction between Ag@I^{3-} and Au@II$^-$ or Pt@II^{2-} compared to the interaction with Ag@II$^-$ or Pd@II^{2-}, which is evident from Figure 4. As the relative intensity in the MS data reflects the abundance of a species, a higher intensity during the fragmentation study suggests that the species Ag@I^{3-} is preferentially retained during the dissociation process, which in turn implies that the interaction between Ag@I^{3-} and Au@II$^-$ or Pt@II^{2-} is energetically more favorable and more difficult to fragment.

Comparison of the Fragmentation Pattern of the Dimers With the Parent NCs. Upon comparison of the fragmentation pattern of the dimeric species with the parent NCs, we noticed significant differences. The dimers, M@III^{3-} (M = Ag and Au), show a very different fragmentation pattern than their parent M@II$^-$ (M = Ag and Au) NCs. However, the fragmentation patterns of the dimers M@IV^{3-} (M = Pd and Pt) were like their parent M@II^{2-} (M = Pd and Pt) NCs.

The fragmentation of Ag@I^{3-} is unique, in comparison to that of M@II^{q-}. The ion $[Ag_{29}L_{12}]^{3-}$ dissociates into $[Ag_{24}L_9]^{2-}$ and $[Ag_5L_3]^-$. The ion $[Ag_{24}L_9]^{2-}$ further loses Ag_2L and $[Ag_3L_2]^-$ to form $[Ag_{22}L_8]^-$ and $[Ag_{21}L_7]^-$. With further increase in CE, the species Ag−S gets detached from the surface, leaving behind the dangling phenyl groups (please recall that the ligand L is a dithiol, and one C−S bond cleavage does not detach it completely from the NC). The detailed fragmentation process of Ag@I^{3-} was discussed in earlier reports.[68,69] We have also observed all types of fragmented species, creating several peaks in the ESI MS as a result of the loss of phenyl rings, S, and Ag. These patterns are shown in Figure 5A.

The fragmentation of $[Ag_{25}L'_{18}]^-$ and $[AuAg_{24}L'_{18}]^-$, both monoanionic species, follows a similar pattern where the fragmentation starts with the loss of neutral $Ag_3L'_3$, generating $[Ag_{22}L'_{15}]^-$ and $[AuAg_{21}L'_{15}]^-$, respectively. The fragmentation of Ag@II$^-$ has been discussed in earlier reports.[68] All the species formed in this dissociation process generate species of 1$^-$ charge state in the lower mass region, from m/z 100 to 1500 in ESI MS, where we observe peaks due to $[AgL'_2]^-$, $[Ag_2L'_3]^-$, $[Ag_3L'_4]^-$, and so on. With a further increase in CE, the higher mass species $[Ag_{22}L'_{15}]^-$ and $[AuAg_{21}L'_{15}]^-$ fragment to give $[Ag_{19}L'_{12}]^-$ and $[AuAg_{18}L'_{12}]^-$, respectively, which further dissociate to give a series of AgL′ loss species. A detailed comparison of the fragmentation pattern of the parent Ag@II$^-$ with the dimer, Ag@III^{3-}, is shown in Figure 5B,C. A similar comparison of the parent Au@II$^-$ with the dimer, Au@III^{3-}, is presented in Figure S24. However, the fragmentation patterns of Pd@II^{2-} and Pt@II^{2-}, which are dianionic species, follow a different pattern than that of Ag@II$^-$, a structural analogue. They first lose smaller monoanionic species $[AgL'_2]^-$, $[Ag_2L'_3]^-$, $[Ag_3L'_4]^-$, and so on to give another series of monoanionic fragments in the higher mass range. Here, in the higher mass range, it appears to be the loss of a series of AgL′ species starting from $[PdAg_{23}L'_{16}]^-$ and $[PtAg_{23}L'_{16}]^-$. Detailed comparisons of the parent Pd@II^{2-} with its dimer, Pd@IV^{3-}, and the parent Pt@II^{2-} with its dimer, Pt@IV^{3-}, are shown in Figures S25 and S26, respectively.

Fragmentation patterns of all dimers have a trend similar to those of the Pd- or Pt-doped M@II^{2-}. It appears that with more energy applied to the trapped ion, it slowly releases the AgL′ fragments from the surface of the dimer, leaving the Ag@I^{3-} intact. The regeneration of Ag@I^{3-} at 40−50 CE shows increased stability of Ag@I^{3-} in the dimer, whereas the trapped ion of the parent Ag@I^{3-} dissociates fully at 30−40 CE (see Figure 5A). The difference in the fragmentation pattern of the dimer from that of the parent Ag@II$^-$ and Au@II$^-$ may imply that dimerization destabilizes the surface AgL′ staples.

DFT Studies of the Dimer Structures. Following the ESI MS analyses, we optimized the structures of the dimers using DFT, for reaction between Ag@I^{3-} and M@II^{q-} (Figure 6). Here, the optimization of all the considered NCs was performed using the projector-augmented-wave (PAW) method, as implemented in the Vienna ab initio simulation package (VASP).[62−64] For the description of the exchange-

https://doi.org/10.1021/acs.jpcc.4c07077
J. Phys. Chem. C XXXX, XXX, XXX−XXX

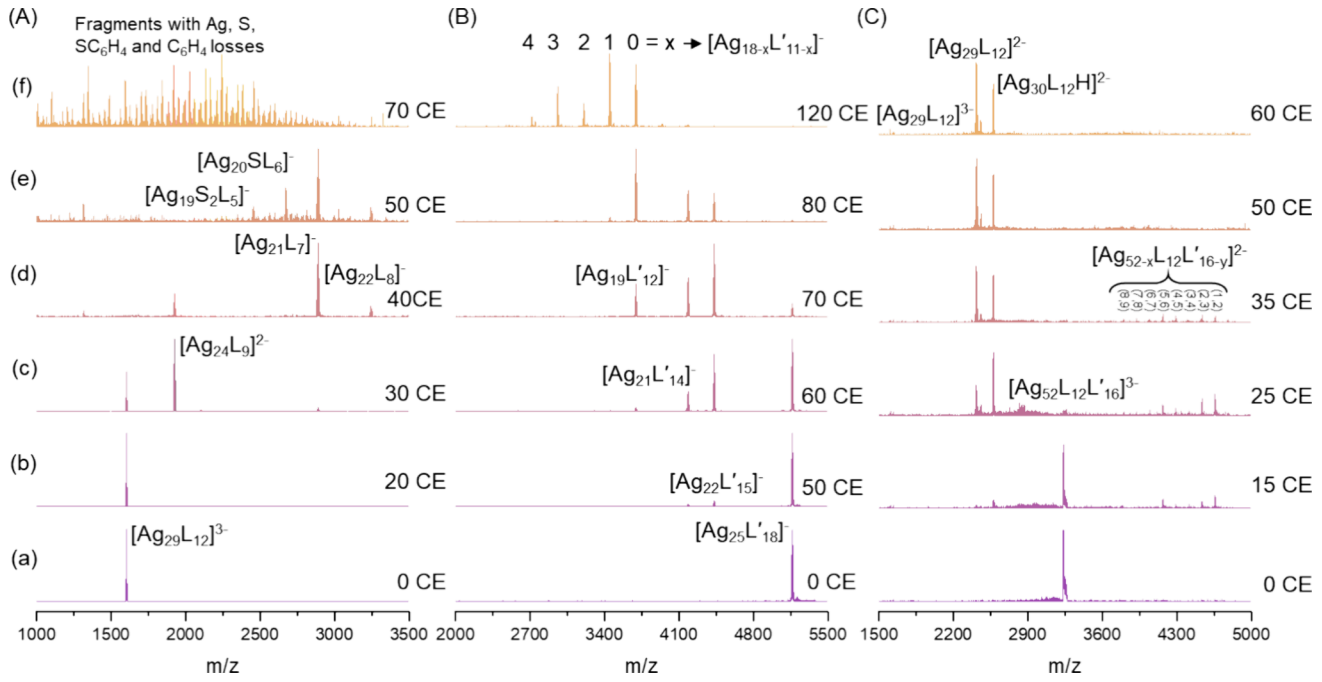

Figure 5. Comparison of the fragmentation patterns of the dimer Ag@III^{3-}, i.e., $[Ag_{53}L_{12}L'_{16}]^{3-}$ with the parent Ag@I^{3-}, i.e., $[Ag_{29}L_{12}]^{3-}$ and Ag@II^{-}, i.e., $[Ag_{25}L'_{18}]^{-}$. (A) MS/MS of $[Ag_{29}L_{12}]^{3-}$ in the window of 0 to 70 CE, (B) MS/MS of $[Ag_{25}L'_{18}]^{-}$ in the window of 0 to 120 CE and (C) MS/MS of $[Ag_{53}L_{12}L'_{16}]^{3-}$ in the window of 0 to 60 CE.

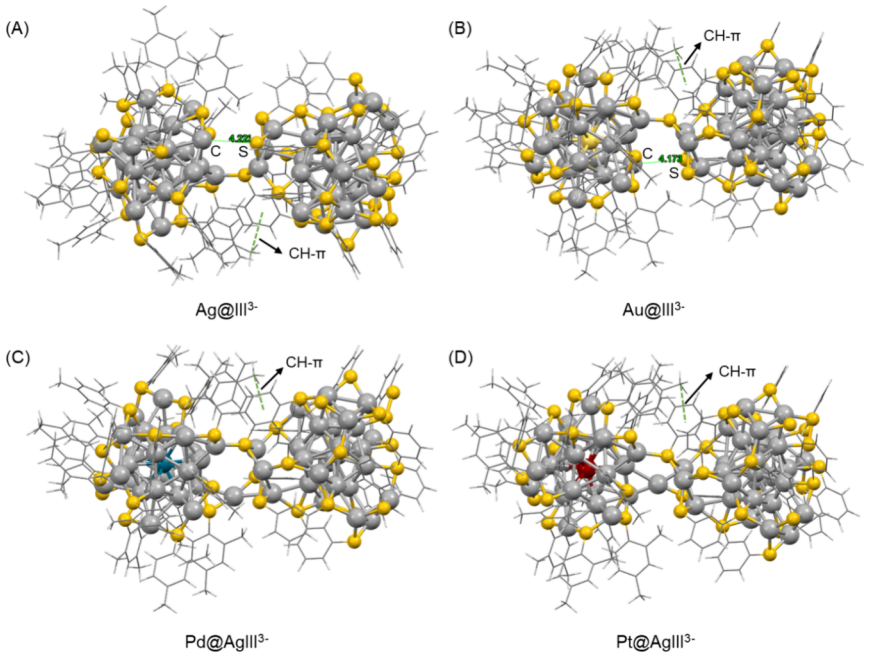

Figure 6. Density functional theory optimized structures for the adducts formed in each of the reactions, shown with supramolecular interaction between the two NCs. (A) Ag@III^{3-}, (B) Au@III^{3-}, (C) Pd@IV^{3-}, and (D) Pt@IV^{3-}. Color code: Ag: gray, Au: light yellow, Pd: greenish blue, Pt: maroon, S: yellow, C and H are shown in wireframe style.

correlation potential, the generalized gradient approximation of Perdew–Burke–Ernzerhof (GGA-PBE) is used.[65] Moreover, to expand the electronic wave function, 470 eV plane wave cutoff energy was used.[62] The convergence criteria are set as 0.05 eV/Å for the force and 1×10^{-2} eV for the electronic energy minimization. For all the calculations, van der Waals correction has been included.

The NCs come closer to each other due to the C–H···π interactions on the surface of the two NCs (Figure 6). To understand the interaction between the two NCs Ag@I^{3-} and Ag@II^{-}, we initially removed two types of $[AgL'_2]^-$ units from the surface of $[Ag_{25}L'_{18}]^-$. One of the two involved two L′ units arranged on the same side of the S–Ag–S (cis arrangement), and the other involved two L′ units on the opposite sides of the S–Ag–S (trans arrangement), which is shown in Figure S27. A stronger interaction was observed between the two NCs Ag@I^{3-} and Ag@II^{-}, by removing the $[AgL'_2]^-$ unit in the trans arrangement, having lower energy.

https://doi.org/10.1021/acs.jpcc.4c07077
J. Phys. Chem. C XXXX, XXX, XXX–XXX

However, we could not obtain a covalently bonded dimer structure from this optimization. A comparison of the energy of interaction between $Ag_{29}L_{12}$ and $Ag_{24}L'_{16}$, with both types of $[AgL'_2]^-$ removals, is provided in Table S1.

To determine the structure of dimer $Ag@III^{3-}$, we first removed the $[AgL'_2]^-$ fragment from the surface of $[Ag_{25}L'_{18}]^-$, to align with the dimer molecular formula $[Ag_{53}L_{12}L'_{16}]^{3-}$ observed in our experiments. In this model, the two L′ units removed were part of different staples in $[Ag_{25}L'_{18}]^-$ that exhibited $\pi\cdots\pi$ stacking interactions. L′ being a monodentate and labile ligand known to undergo exchange during solution phase reactions of NCs.[37,70] However, the ligand L, protecting $[Ag_{29}L_{12}]^{3-}$ NC, is a highly stable bidentate ligand that is difficult to exchange/remove under solution phase conditions,[40,38] which is also evident from our fragmentation studies on the dimers. So, next, we connected the two sulfur atoms from the distinct L units on the $[Ag_{29}L_{12}]^{3-}$ surface to the vacant sulfur positions on $Ag_{24}L'_{16}$, forming the $[Ag_{53}L_{12}L'_{16}]^{3-}$ structure (see Figure S28). This structure was taken as the starting structure for the dimer formed in view of the most prominent peak observed in the ESI MS study. To form the $Au@III^{3-}$ structure, the central Ag atom in $Ag@II^-$ was replaced with Au and to get the $M@IV^{3-}$ structure, the one extra Ag atom (from $Ag@III^{3-}$) was placed back in its original position, and the structure was optimized. All of these dimer structures were optimized using DFT calculations and are shown in Figure 6. The optimized structures of dimers having new strong covalent bonds between the two NCs indicate that stable dimers can form between $Ag@I^{3-}$ and $M@II^{q-}$ while maintaining their original configurations. During dimer optimization, the newly formed Ag−S bonds at the interface of the two NCs were found to range between 2.4 and 2.5 Å. These bonds rearranged into a stable configuration, stabilized by C−H$\cdots\pi$ interactions between the L and L′ ligands from $Ag@I^{3-}$ and $M@II^{q-}$ NC, respectively, as shown in Figure 6. From these calculations, we have also obtained the optimized energy for all of the dimeric species. All these calculations were performed using DFT, as implemented in VASP. The energy comparison between dimers of the same nuclearities indicates that $Au@III^{3-}$ was more stable compared to $Ag@III^{3-}$, and $Pt@IV^{3-}$ was more stable compared to $Pd@IV^{3-}$. The optimized energies for all the dimers are given in Table S2 and the relative energy comparison is given in Table 1.

Table 1. Relative Energy of $Au@III^{3-}$ in Comparison to $Ag@III^{3-}$ and Relative Energy of $Pt@IV^{3-}$ in Comparison to $Pd@IV^{3-}$

dimer	relative energy in comparison to $Ag@III^{3-}$ (eV)	dimer	relative energy in comparison to $Pd@IV^{3-}$ (eV)
$Ag@III^{3-}$	0	$Pd@IV^{3-}$	0
$Au@III^{3-}$	−1.05	$Pt@IV^{3-}$	−0.35

We have also calculated the average distances of all the Ag atoms present in the Ag_{13} core as well as the distances of Ag in the staples on the surface of both the NCs from the central atom M, in the optimized dimer structures (see Table S3). In the case of $Pd@IV^{3-}$ and $Pt@IV^{3-}$ dimers, the distance between M-Ag in $MAg_{24}L'_{16}$ is shorter in both the MAg_{12} core and the Ag in the staple, compared to those of $Ag@III^{3-}$ and its $Au@III^{3-}$ dimers. This can be due to extra Ag atoms in both $Pd@IV^{3-}$ and $Pt@IV^{3-}$ dimers which increases the argentophilic interactions causing contraction of their MAg_{12} core and the Ag-ligand staple.[71−73] The average distances of Ag atoms from the center show that the doping of Pd and Pt in $M@II^{2-}$ results in the silver atoms being held more closely to the center than the doping of Ag and Au in $M@II^-$. However, no significant changes were observed in the distances of Ag−Ag from the center to the Ag_{13} core and Ag in the staple of the $Ag@I^{3-}$ NC upon dimer formation. These calculations indicate that among the formed dimers, $Au@III^{3-}$ is more stable compared to $Ag@III^{3-}$, and similarly, $Pt@IV^{3-}$ is more stable compared to $Pd@IV^{3-}$ which also supports the experimental findings (Figure 4). Also, we can conclude that alloying enhances the stability of the dimers.

Dimer Formation in the Case of $M@I^{p-}$ and $Ag@II^-$. To further explore the dimer formation between such NCs which are homometallic, heteroligand, and selectively doped, we performed a reaction between $Au@I^{3-}$ and $Ag@II^-$ and studied its MS. To our surprise, this gave us the same dimeric species in the ESI MS analysis, in the m/z 3000 to 3500 range (details are in Figure S29). A comparison of the dimeric species formed in the case of the reaction between $Ag@I^{3-}$ and $Au@II^-$ with $Au@I^{3-}$ and $Ag@II^-$ is shown in Figure 7. Which

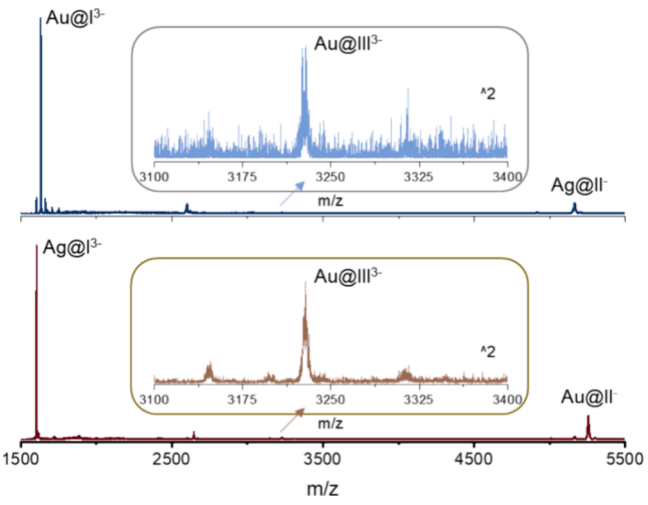

Figure 7. Comparison of the $Ag@I^{3-}$ + $Au@II^-$ reaction with the $Au@I^{3-}$ + $Ag@II^-$ reaction, giving the same dimeric species.

means that the central atom in the parent NCs only influences the stability of the dimers formed but does not exchange between the NCs during the reaction. We also performed a similar reaction between $Pd@I^{4-}$ and $Pt@I^{4-}$ with $Ag@II^-$, which gave similar dimeric species, as shown in Figures S30 and S31. Finally, we reacted $Au@I^{3-}$ and $Au@II^-$, which also formed dimeric species in the m/z 3000 to 3500 region (Figure S32), confirming that dimer formation is generic for these NCs.

CONCLUSIONS

Atomically precise noble metal nanoclusters $[Ag_{29}(1,3\text{-}BDT)_{12}]^{3-}$ ($Ag@I^{3-}$) and center-doped $[MAg_{24}(2,4\text{-}DMBT)_{18}]^{q-}$ ($M@II^{q-}$) (q = 1 for M = Ag/ Au, and q = 2 for M = Pd/ Pt) react in solution forming dimers, which were detected for a period of 48 h. The dimeric species formed were $[MAg_{53-x}L_{12}L'_{18-y}]^{3-}$ ($x \geq 0$ and $y \geq 0$), with varying central

https://doi.org/10.1021/acs.jpcc.4c07077
J. Phys. Chem. C XXXX, XXX, XXX−XXX

atoms, M = Ag/Au/Pd/Pt. These dimers were detected by electrospray ionization mass spectrometry. Such stable dimers—not transient ones—have been reported for the first time during intercluster reactions. The dimers have 16 electrons in their valence shells and appear to be stable electronically. UV/vis spectroscopy provided complementary information about the dimers. Quantum chemical calculations provided insights into the structures of the dimers that were brought together by ligand interactions, ultimately leading to strong metal−ligand bonding at the interface.

■ ASSOCIATED CONTENT

Supporting Information

The Supporting Information is available free of charge at https://pubs.acs.org/doi/10.1021/acs.jpcc.4c07077.

Instrumentation, characterization of parent NCs, detailed MS studies for all the reactions, stability of each dimer using UV/vis and MS studies, detailed fragmentation studies for dimers and parent NCs, DFT calculations, and other relevant data (PDF)

■ AUTHOR INFORMATION

Corresponding Authors

Biswarup Pathak − *Department of Chemistry, IIT Indore, Indore 453552, India;* orcid.org/0000-0002-9972-9947; Email: biswarup@iiti.ac.in

Thalappil Pradeep − *DST Unit of Nanoscience (DSTUNS) and Thematic Unit of Excellence (TUE), Department of Chemistry, IIT Madras, Chennai 600036, India; International Centre for Clean Water, IIT Madras Research Park, Chennai 600113, India;* orcid.org/0000-0003-3174-534X; Email: pradeep@iitm.ac.in

Authors

Swetashree Acharya − *DST Unit of Nanoscience (DSTUNS) and Thematic Unit of Excellence (TUE), Department of Chemistry, IIT Madras, Chennai 600036, India*

Jayoti Roy − *DST Unit of Nanoscience (DSTUNS) and Thematic Unit of Excellence (TUE), Department of Chemistry, IIT Madras, Chennai 600036, India*

Diptendu Roy − *Department of Chemistry, IIT Indore, Indore 453552, India;* orcid.org/0000-0001-7718-3018

Complete contact information is available at: https://pubs.acs.org/10.1021/acs.jpcc.4c07077

Notes

The authors declare no competing financial interest.

■ ACKNOWLEDGMENTS

S.A. acknowledges support from the Prime Minister's Research Fellowship (PMRF). J.R. is grateful to IIT Madras for financial assistance. D.R. acknowledges MHRD for his research fellowship. D.R. and B.P. acknowledge the lab and computer facilities provided by IIT Indore. This work was funded by the following organizations: DST-SERB (Project Number: CRG/2022/000836), New Delhi, BRNS (Project Number: 2023-BRNS/12356), and CSIR (project 01(3046)/21/EMR-II). T.P. acknowledges funding through the Centre of Excellence (CoE) on Molecular Materials and Functions supported by the Institute of Eminence program. The Science and Engineering Research Board (SERB), India, is also acknowledged for funds provided through the SPR/2021/000439 research grant and a JC Bose Fellowship awarded to T.P. S.A. thanks Dr. Papri Chakraborty and Dr. Esma Khatun for their valuable inputs related to this work.

■ REFERENCES

(1) Jin, R.; Zeng, C.; Zhou, M.; Chen, Y. Atomically Precise Colloidal Metal Nanoclusters and Nanoparticles: Fundamentals and Opportunities. *Chem. Rev.* **2016**, *116* (18), 10346−10413.

(2) Chakraborty, I.; Pradeep, T. Atomically Precise Clusters of Noble Metals: Emerging Link between Atoms and Nanoparticles. *Chem. Rev.* **2017**, *117* (12), 8208−8271.

(3) Pradeep, T. Chapter 1 - Atomically Precise Clusters of Noble Metals: An Introduction. In *Atomically Precise Metal Nanoclusters*; Pradeep, T., Ed.; Elsevier, 2023; 1−5.

(4) Sooraj, B. N. S.; Pradeep, T. Chapter 4 - Optical Properties of Metal Clusters. In *Atomically Precise Metal Nanoclusters*; Pradeep, T., Ed.; Elsevier, 2023; 83−101.

(5) Chakraborty, I.; Udayabhaskararao, T.; Pradeep, T. Luminescent Sub-Nanometer Clusters for Metal Ion Sensing: A New Direction in Nanosensors. *J. Hazard. Mater.* **2012**, *211−212*, 396−403.

(6) Yuan, X.; Luo, Z.; Yu, Y.; Yao, Q.; Xie, J. Luminescent Noble Metal Nanoclusters as an Emerging Optical Probe for Sensor Development. *Chem.−Asian J.* **2013**, *8* (5), 858−871.

(7) Du, Y.; Sheng, H.; Astruc, D.; Zhu, M. Atomically Precise Noble Metal Nanoclusters as Efficient Catalysts: A Bridge between Structure and Properties. *Chem. Rev.* **2020**, *120* (2), 526−622.

(8) Kawawaki, T.; Okada, T.; Hirayama, D.; Negishi, Y. Atomically Precise Metal Nanoclusters as Catalysts for Electrocatalytic CO 2 Reduction. *Green Chem.* **2024**, *26* (1), 122−163.

(9) Mathew, A.; Pradeep, T. Noble Metal Clusters: Applications in Energy, Environment, and Biology. *Part. Part. Syst. Charact.* **2014**, *31* (10), 1017−1053.

(10) Yang, J.; Yang, F.; Zhang, C.; He, X.; Jin, R. Metal Nanoclusters as Biomaterials for Bioapplications: Atomic Precision as the Next Goal. *ACS Mater. Lett.* **2022**, *4* (7), 1279−1296.

(11) Fang, J.; Zhang, B.; Yao, Q.; Yang, Y.; Xie, J.; Yan, N. Recent Advances in the Synthesis and Catalytic Applications of Ligand-Protected, Atomically Precise Metal Nanoclusters. *Coord. Chem. Rev.* **2016**, *322*, 1−29.

(12) Du, X.; Jin, R. Atomically Precise Metal Nanoclusters for Catalysis. *ACS Nano* **2019**, *13* (7), 7383−7387.

(13) Yuan, X.; Zhu, M. Recent Advances in Atomically Precise Metal Nanoclusters for Electrocatalytic Applications. *Inorg. Chem. Front.* **2023**, *10* (14), 3995−4007.

(14) Natarajan, G.; Mathew, A.; Negishi, Y.; Whetten, R. L.; Pradeep, T. A Unified Framework for Understanding the Structure and Modifications of Atomically Precise Monolayer Protected Gold Clusters. *J. Phys. Chem. C* **2015**, *119* (49), 27768−27785.

(15) Aikens, C. M. Electronic and Geometric Structure, Optical Properties, and Excited State Behavior in Atomically Precise Thiolate-Stabilized Noble Metal Nanoclusters. *Acc. Chem. Res.* **2018**, *51* (12), 3065−3073.

(16) Wang, S.; Song, Y.; Jin, S.; Liu, X.; Zhang, J.; Pei, Y.; Meng, X.; Chen, M.; Li, P.; Zhu, M. Metal Exchange Method Using Au25 Nanoclusters as Templates for Alloy Nanoclusters with Atomic Precision. *J. Am. Chem. Soc.* **2015**, *137* (12), 4018−4021.

(17) Bootharaju, M. S.; Joshi, C. P.; Parida, M. R.; Mohammed, O. F.; Bakr, O. M. Templated Atom-Precise Galvanic Synthesis and Structure Elucidation of a [Ag24Au(SR)18]−Nanocluster. *Angew. Chem., Int. Ed.* **2016**, *55* (3), 922−926.

(18) Ghosh, A.; Mohammed, O. F.; Bakr, O. M. Atomic-Level Doping of Metal Clusters. *Acc. Chem. Res.* **2018**, *51* (12), 3094−3103.

(19) Song, Y.; Abroshan, H.; Chai, J.; Kang, X.; Kim, H. J.; Zhu, M.; Jin, R. Molecular-like Transformation from PhSe-Protected Au25 to Au23 Nanocluster and Its Application. *Chem. Mater.* **2017**, *29* (7), 3055−3061.

(20) Salassa, G.; Sels, A.; Mancin, F.; Bürgi, T. Dynamic Nature of Thiolate Monolayer in Au25(SR)18 Nanoclusters. *ACS Nano* **2017**, *11* (12), 12609−12614.
(21) Zheng, K.; Fung, V.; Yuan, X.; Jiang, D.; Xie, J. Real Time Monitoring of the Dynamic Intracluster Diffusion of Single Gold Atoms into Silver Nanoclusters. *J. Am. Chem. Soc.* **2019**, *141* (48), 18977−18983.
(22) Chakraborty, A.; Stanley, M. M.; Mondal, B.; Nonappa; Bodiuzzaman, M.; Chakraborty, P.; Kannan, M. P.; Pradeep, T. Tunable Reactivity of Silver Nanoclusters: A Facile Route to Synthesize a Range of Bimetallic Nanostructures. *Nanoscale* **2023**, *15* (6), 2690−2699.
(23) Niihori, Y.; Hossain, S.; Sharma, S.; Kumar, B.; Kurashige, W.; Negishi, Y. Understanding and Practical Use of Ligand and Metal Exchange Reactions in Thiolate-Protected Metal Clusters to Synthesize Controlled Metal Clusters. *Chem. Rec.* **2017**, *17* (5), 473−484.
(24) Yan, J.; Teo, B. K.; Zheng, N. Surface Chemistry of Atomically Precise Coinage−Metal Nanoclusters: From Structural Control to Surface Reactivity and Catalysis. *Acc. Chem. Res.* **2018**, *51* (12), 3084−3093.
(25) Chakraborty, P.; Nag, A.; Chakraborty, A.; Pradeep, T. Approaching Materials with Atomic Precision Using Supramolecular Cluster Assemblies. *Acc. Chem. Res.* **2019**, *52* (1), 2−11.
(26) Wei, X.; Kang, X.; Yuan, Q.; Qin, C.; Jin, S.; Wang, S.; Zhu, M. Capture of Cesium Ions with Nanoclusters: Effects on Inter- and Intramolecular Assembly. *Chem. Mater.* **2019**, *31* (13), 4945−4952.
(27) Yao, Q.; Wu, Z.; Liu, Z.; Lin, Y.; Yuan, X.; Xie, J. Molecular Reactivity of Thiolate-Protected Noble Metal Nanoclusters: Synthesis, Self-Assembly, and Applications. *Chem. Sci.* **2021**, *12* (1), 99−127.
(28) Wei, X.; Kang, X.; Zuo, Z.; Song, F.; Wang, S.; Zhu, M. Hierarchical Structural Complexity in Atomically Precise Nanocluster Frameworks. *Natl. Sci. Rev.* **2021**, *8* (3), No. nwaa077.
(29) Wei, X.; Chu, K.; Adsetts, J. R.; Li, H.; Kang, X.; Ding, Z.; Zhu, M. Nanocluster Transformation Induced by SbF6−Anions toward Boosting Photochemical Activities. *J. Am. Chem. Soc.* **2022**, *144* (44), 20421−20433.
(30) Shen, H.; Xu, J.; Fu, Z.; Wei, X.; Kang, X.; Shi, W.; Zhu, M. Photoluminescence Quenching of Hydrophobic Ag29 Nanoclusters Caused by Molecular Decoupling during Aqueous Phase Transfer and EmissionRecovery through Supramolecular Recoupling. *Angew. Chem., Int. Ed.* **2024**, *63* (12), No. e202317995.
(31) Wilcoxon, J. P.; Abrams, B. L. Synthesis, Structure and Properties of Metal Nanoclusters. *Chem. Soc. Rev.* **2006**, *35* (11), 1162−1194.
(32) Qian, H.; Zhu, M.; Wu, Z.; Jin, R. Quantum Sized Gold Nanoclusters with Atomic Precision. *Acc. Chem. Res.* **2012**, *45* (9), 1470−1479.
(33) Lu, Y.; Chen, W. Sub-Nanometre Sized Metal Clusters: From Synthetic Challenges to the Unique Property Discoveries. *Chem. Soc. Rev.* **2012**, *41* (9), 3594−3623.
(34) Yao, Q.; Chen, T.; Yuan, X.; Xie, J. Toward Total Synthesis of Thiolate-Protected Metal Nanoclusters. *Acc. Chem. Res.* **2018**, *51* (6), 1338−1348.
(35) Kang, X.; Li, Y.; Zhu, M.; Jin, R. Atomically Precise Alloy Nanoclusters: Syntheses, Structures, and Properties. *Chem. Soc. Rev.* **2020**, *49* (17), 6443−6514.
(36) Yang, J.; Jin, R. New Advances in Atomically Precise Silver Nanoclusters. *ACS Mater. Lett.* **2019**, *1* (4), 482−489.
(37) Krishnadas, K. R.; Ghosh, A.; Baksi, A.; Chakraborty, I.; Natarajan, G.; Pradeep, T. Intercluster Reactions between $Au_{25}(SR)_{18}$ and $Ag_{44}(SR)_{30}$. *J. Am. Chem. Soc.* **2016**, *138* (1), 140−148.
(38) Khatun, E.; Chakraborty, P.; Jacob, B. R.; Paramasivam, G.; Bodiuzzaman, M.; Dar, W. A.; Pradeep, T. Intercluster Reactions Resulting in Silver-Rich Trimetallic Nanoclusters. *Chem. Mater.* **2020**, *32* (1), 611−619.
(39) Krishnadas, K. R.; Baksi, A.; Ghosh, A.; Natarajan, G.; Pradeep, T. Structure-Conserving Spontaneous Transformations between Nanoparticles. *Nat. Commun.* **2016**, *7* (1), 13447.
(40) Ghosh, A.; Ghosh, D.; Khatun, E.; Chakraborty, P.; Pradeep, T. Unusual Reactivity of Dithiol Protected Clusters in Comparison to Monothiol Protected Clusters: Studies Using $Ag_{51}(BDT)_{19}(TPP)_{3}$ and $Ag_{29}(BDT)_{12}(TPP)_{4}$. *Nanoscale* **2017**, *9* (3), 1068−1077.
(41) Krishnadas, K. R.; Baksi, A.; Ghosh, A.; Natarajan, G.; Som, A.; Pradeep, T. Interparticle Reactions: An Emerging Direction in Nanomaterials Chemistry. *Acc. Chem. Res.* **2017**, *50* (8), 1988−1996.
(42) Krishnadas, K. R.; Baksi, A.; Ghosh, A.; Natarajan, G.; Pradeep, T. Manifestation of Geometric and Electronic Shell Structures of Metal Clusters in Intercluster Reactions. *ACS Nano* **2017**, *11* (6), 6015−6023.
(43) Krishnadas, K. R.; Natarajan, G.; Baksi, A.; Ghosh, A.; Khatun, E.; Pradeep, T. Metal−Ligand Interface in the Chemical Reactions of Ligand-Protected Noble Metal Clusters. *Langmuir* **2019**, *35* (35), 11243−11254.
(44) Neumaier, M.; Baksi, A.; Weis, P.; Schneider, E. K.; Chakraborty, P.; Hahn, H.; Pradeep, T.; Kappes, M. M. Kinetics of Intercluster Reactions between Atomically Precise Noble Metal Clusters $[Ag_{25}(DMBT)_{18}]^{-}$ and $[Au_{25}(PET)_{18}]^{-}$ in Room Temperature Solutions. *J. Am. Chem. Soc.* **2021**, *143* (18), 6969−6980.
(45) Huang, B.; Pei, Y. On the Mechanism of Inter-Cluster Alloying Reactions: Two-Stage Metal Exchange of $[Au_{25}(PET)_{18}]^{-}$ and $[Ag_{25}(DMBT)_{18}]^{-}$ Clusters. *J. Mater. Chem. A* **2020**, *8* (20), 10242−10251.
(46) Bose, P.; Chakraborty, P.; Mohanty, J. S.; Nonappa; Chowdhuri, A. R.; Khatun, E.; Ahuja, T.; Mahendranath, A.; Pradeep, T. Atom Transfer between Precision Nanoclusters and Polydispersed Nanoparticles: A Facile Route for Monodisperse Alloy Nanoparticles and Their Superstructures. *Nanoscale* **2020**, *12* (43), 22116−22128.
(47) Roy, J.; Mondal, B.; Vishwakarma, G.; Nonappa; Sridharan, N. V.; Krishnamurthi, P.; Pradeep, T. Dissociative Reactions of [Au25(SR)18]−at Copper Oxide Nanoparticles and Formation of Aggregated Nanostructures. *Nanoscale* **2023**, *15* (18), 8225−8234.
(48) Bose, P.; Roy, J.; Khokhar, V.; Mondal, B.; Natarajan, G.; Manna, S.; Yadav, V.; Nyayban, A.; Yamijala, S. S. R. K. C.; Nonappa.; et al. Interparticle Antigalvanic Reactions of Atomically Precise Silver Nanoclusters with Plasmonic Gold Nanoparticles: Interfacial Control of Atomic Exchange. *Chem. Mater.* **2024**, *36* (15), 7581−7594.
(49) Kazan, R.; Müller, U.; Bürgi, T. Doping of Thiolate Protected Gold Clusters through Reaction with Metal Surfaces. *Nanoscale* **2019**, *11* (6), 2938−2945.
(50) Chakraborty, P.; Bose, P.; Roy, J.; Nag, A.; Mondal, B.; Chakraborty, A.; Pradeep, T. Isotopic Exchange of Atomically Precise Nanoclusters with Materials of Varying Dimensions: From Nanoscale to Bulk. *J. Phys. Chem. C* **2021**, *125* (29), 16110−16117.
(51) Kim, M.; Weerawardene, K. L. D. M.; Choi, W.; Han, S. M.; Paik, J.; Kim, Y.; Choi, M.-G.; Aikens, C. M.; Lee, D. Insights into the Metal-Exchange Synthesis of MAg24(SR)18 (M = Ni, Pd, Pt) Nanoclusters. *Chem. Mater.* **2020**, *32* (23), 10216−10226.
(52) Tang, L.; Kang, X.; Wang, X.; Zhang, X.; Yuan, X.; Wang, S. Dynamic Metal Exchange between a Metalloid Silver Cluster and Silver(I) Thiolate. *Inorg. Chem.* **2021**, *60* (5), 3037−3045.
(53) Bose, P.; Ramankutty, K. K.; Chakraborty, P.; Khatun, E.; Pradeep, T. A Concise Guide to Chemical Reactions of Atomically Precise Noble Metal Nanoclusters. *Nanoscale* **2024**, *16* (4), 1446−1470.
(54) Chakraborty, P.; Nag, A.; Natarajan, G.; Bandyopadhyay, N.; Paramasivam, G.; Panwar, M. K.; Chakrabarti, J.; Pradeep, T. Rapid Isotopic Exchange in Nanoparticles. *Sci. Adv.* **2019**, *5* (1), No. eaau7555.
(55) Baksi, A.; Chakraborty, P.; Bhat, S.; Natarajan, G.; Pradeep, T. [Au25(SR)18]22−: A Noble Metal Cluster Dimer in the Gas Phase. *Chem. Commun.* **2016**, *52* (54), 8397−8400.

https://doi.org/10.1021/acs.jpcc.4c07077
J. Phys. Chem. C XXXX, XXX, XXX−XXX

(56) Swierczewski, M.; Cousin, F.; Banach, E.; Rosspeintner, A.; Lawson Daku, L. M.; Ziarati, A.; Kazan, R.; Jeschke, G.; Azoulay, R.; Lee, L.-T.; et al. Exceptionally Stable Dimers and Trimers of Au25 Clusters Linked with a Bidentate Dithiol: Synthesis, Structure and Chirality Study. *Angew. Chem., Int. Ed.* **2023**, *62* (16), No. e202215746.
(57) Chakraborty, P.; Baksi, A.; Mudedla, S. K.; Nag, A.; Paramasivam, G.; Subramanian, V.; Pradeep, T. Understanding Proton Capture and Cation-Induced Dimerization of [Ag29(BDT)-12]3−Clusters by Ion Mobility Mass Spectrometry. *Phys. Chem. Chem. Phys.* **2018**, *20* (11), 7593−7603.
(58) Joshi, C. P.; Bootharaju, M. S.; Alhilaly, M. J.; Bakr, O. M. $[Ag_{25}(SR)_{18}]^-$: The "Golden" Silver Nanoparticle. *J. Am. Chem. Soc.* **2015**, *137* (36), 11578−11581.
(59) Yan, J.; Su, H.; Yang, H.; Malola, S.; Lin, S.; Häkkinen, H.; Zheng, N. Total Structure and Electronic Structure Analysis of Doped Thiolated Silver [MAg24(SR)18]2−(M = Pd, Pt) Clusters. *J. Am. Chem. Soc.* **2015**, *137* (37), 11880−11883.
(60) AbdulHalim, L. G.; Bootharaju, M. S.; Tang, Q.; Del Gobbo, S.; AbdulHalim, R. G.; Eddaoudi, M.; Jiang, D.; Bakr, O. M. $Ag_{29}(BDT)_{12}(TPP)_4$: A Tetravalent Nanocluster. *J. Am. Chem. Soc.* **2015**, *137* (37), 11970−11975.
(61) Zeng, C. Precision at the Nanoscale: On the Structure and Property Evolution of Gold Nanoclusters. *Pure Appl. Chem.* **2018**, *90* (9), 1409−1427.
(62) Kresse, G.; Furthmüller, J. Efficient Iterative Schemes for Ab Initio Total-Energy Calculations Using a Plane-Wave Basis Set. *Phys. Rev. B* **1996**, *54* (16), 11169−11186.
(63) Kresse, G.; Joubert, D. From Ultrasoft Pseudopotentials to the Projector Augmented-Wave Method. *Phys. Rev. B* **1999**, *59* (3), 1758−1775.
(64) Blöchl, P. E. Projector Augmented-Wave Method. *Phys. Rev. B* **1994**, *50* (24), 17953−17979.
(65) Perdew, J. P.; Chevary, J. A.; Vosko, S. H.; Jackson, K. A.; Pederson, M. R.; Singh, D. J.; Fiolhais, C. Atoms, Molecules, Solids, and Surfaces: Applications of the Generalized Gradient Approximation for Exchange and Correlation. *Phys. Rev. B* **1992**, *46* (11), 6671−6687.
(66) Nag, A.; Chakraborty, P.; Natarajan, G.; Baksi, A.; Mudedla, S. K.; Subramanian, V.; Pradeep, T. Bent Keto Form of Curcumin, Preferential Stabilization of Enol by Piperine, and Isomers of Curcumin∩Cyclodextrin Complexes: Insights from Ion Mobility Mass Spectrometry. *Anal. Chem.* **2018**, *90* (15), 8776−8784.
(67) Xia, H.; Attygalle, A. B. Effect of Electrospray Ionization Source Conditions on the Tautomer Distribution of Deprotonated P-Hydroxybenzoic Acid in the Gas Phase. *Anal. Chem.* **2016**, *88* (11), 6035−6043.
(68) Chakraborty, P.; Baksi, A.; Khatun, E.; Nag, A.; Ghosh, A.; Pradeep, T. Dissociation of Gas Phase Ions of Atomically Precise Silver Clusters Reflects Their Solution Phase Stability. *J. Phys. Chem. C* **2017**, *121* (20), 10971−10981.
(69) Chakraborty, P.; Malola, S.; Neumaier, M.; Weis, P.; Häkkinen, H.; Kappes, M. M. Elucidating the Structures of Intermediate Fragments during Stepwise Dissociation of Monolayer-Protected Silver Clusters. *Angew. Chem.* **2023**, *135* (29), No. e202305836.
(70) Bose, P.; Roy, J.; Khokhar, V.; Mondal, B.; Natarajan, G.; Manna, S.; Yadav, V.; Nyayban, A.; Yamijala, S. S. R. K. C.; Nonappa; Pradeep, T. Interparticle Antigalvanic Reactions of Atomically Precise Silver Nanoclusters with Plasmonic Gold Nanoparticles: Interfacial Control of Atomic Exchange. *Chem. Mater.* **2024**, *36* (15), 7581−7594.
(71) Koskinen, L.; Jääskeläinen, S.; Oresmaa, L.; Haukka, M. Argentophilic Interactions in Multinuclear Ag Complexes of Imidazole Containing Schiff Bases. *CrystEngComm* **2012**, *14* (10), 3509−3514.
(72) Schmidbaur, H.; Schier, A. Argentophilic Interactions. *Angew. Chem., Int. Ed.* **2015**, *54* (3), 746−784.
(73) Alhilaly, M. J.; Huang, R.-W.; Naphade, R.; Alamer, B.; Hedhili, M. N.; Emwas, A.-H.; Maity, P.; Yin, J.; Shkurenko, A.; Mohammed, O. F.; et al. Assembly of Atomically Precise Silver Nanoclusters into Nanocluster-Based Frameworks. *J. Am. Chem. Soc.* **2019**, *141* (24), 9585−9592.

https://doi.org/10.1021/acs.jpcc.4c07077
J. Phys. Chem. C XXXX, XXX, XXX−XXX